Full length article

The N-body interatomic potentials for molecular dynamics simulations of diffusion in C15 Cr$_2$Ta Laves phase

D.O. Poletaev [a,b,d,*], A.G. Lipnitskii [b,c], V.N. Maksimenko [b,c], Yu.R. Kolobov [c], A.G. Beresnev [e], M.S. Gusakov [e]

[a] *Materials Discovery Laboratory, Skolkovo Institute of Science and Technology, Moscow, Russia*
[b] *The Center of Nanostructured Materials and Nanotechnologies, Belgorod State University, Belgorod, Russia*
[c] *Institute of Problems of Chemical Physics (IPCP), Russian Academy of Sciences, Chernogolovka, Moscow, Russia*
[d] *Frank Laboratory of Neutron Physics, Joint Institute for Nuclear Research, Dubna, Russia*
[e] *JSC Komposit, Korolev, Moscow oblast, Russia*

A B S T R A C T

In this work, the interatomic potentials for modeling diffusion in the C15 Cr$_2$Ta Laves phase were constructed within the N-body approach. The potential for Ta–Ta interactions reproduces the lattice parameter, cohesive energy, elastic constants, equation of state, thermal expansion, point defect energies, and phonon dispersion of body-centered cubic Ta in qualitative agreement with density functional theory (DFT) data and almost quantitative agreement with available experimental data in the temperature range of stability of C15 Cr$_2$Ta Laves phase. The potential for Cr–Ta interactions reproduces the elastic constants, point defect properties, equilibrium volumes, and formation enthalpies of Cr–Ta structures in qualitative agreement with DFT data. Also, it reproduces the lattice stability and high-temperature formation enthalpy of C15 Cr$_2$Ta Laves phase in very close agreement with the available experimental data. The calculations of diffusion coefficients with constructed potentials showed that diffusion in C15 Cr$_2$Ta lattice is governed by Cr atoms which cannot move without creation of vacancies. The constructed potentials can be used in further investigations of diffusion processes in Cr–Ta phases at temperatures up to 2000 K, while the obtained results on diffusion coefficients in C15 Cr$_2$Ta Laves phase would be useful in the rational design of Cr–Ta based alloys.

1. Introduction

The Cr$_2$Ta intermetallics attract an interest in aerospace and high-temperature applications due to its low density, high melting temperature, and high oxidation resistance. In dependence on the temperature, the Cr$_2$Ta can exist in C14, C15, or C36 crystal structures [1–5], among which the cubic C15 is the most stable one in the temperature range from 0 to 1963 K [3].

Despite the extensive experimental [4–15], theoretical [16–18], and theoretical-experimental [2,19] investigations of Cr$_2$Ta phase stability [2,15], properties [16–18], influence on microstructure [4,5,7,9,10, 15,19], mechanical behavior [5,10,14], and oxidation resistance [6,8,9, 19] of binary Cr–Ta [4,7] and ternary Cr-Ta-X (where X = Mo [5,13], Al [5], Si [5,9,10,14], Fe [11], Ru [12], or V [15]) alloys there are several aspects that need to be additionally explored with atomistic simulation methods. Among them there are coefficients and mechanisms of diffusion in Cr$_2$Ta Laves phases. Knowledge of the diffusion behavior of intermetallics is important in the context of their high-temperature structural applications because their high-temperature strength is limited by diffusion-controlled creep processes.

There are very few experimental investigations of diffusion in Laves phases at all. In particular, there are only two investigations of inter-diffusion for Cr–Ta alloys [20,21] from which the experimentally based diffusion coefficients in solid solutions and intermediate Cr$_2$Ta phase are obtained at 2128 K, 2165 K [20] and 1373 K [21]. However, in the mentioned experiments [20,21] the diffusion coefficients only in the hexagonal C14 Cr$_2$Ta phase are most probably extracted because at temperatures higher than 2000 K the C14 phase is the stablest at Cr$_2$Ta composition [3] while at temperatures around 1373 K or lower the C14 phase is a primarily formed phase [4,7] due to kinetic reasons. Thus, there is no information in the literature about diffusion in the cubic C15 Cr$_2$Ta phase. Meanwhile, the knowledge of the diffusion properties of C15 Cr$_2$Ta phase and understanding the self-diffusion mechanisms in it is also important because namely, this phase is the most stable one in many Cr–Ta based alloys.

Since the diffusion in metals and alloys is the atomistic process, one of the best ways to get insight into its mechanisms is to conduct the atomic scale simulations with different model samples employing molecular dynamics (MD). For example, the molecular dynamics simulations allowed to establish the leading mechanism of the self-diffusion phenomena in Ni_2Y Laves phase [22].

The bottleneck in implementing such a scheme for Cr–Ta alloys was the unavailability of appropriate interatomic potentials. In this work, we construct such potentials within the N-body approach [23,24] and use them to disclose the self-diffusion mechanisms and derive the diffusion coefficients in cubic C15 Cr_2Ta Laves phase from the analysis of results of molecular dynamics simulations.

2. Methodology

2.1. Interatomic potentials

Within the N-body approach [23,24] the potential energy of a system of atoms is described by the following expression:

$$E_{pot} = \sum_{i<j}^{N} \Phi(R_{ji}) + \sum_{i}^{N} \sum_{k<j\neq i}^{N} \sum_{p,q}^{n_3} g^{pq}(cos(\theta_{jik}))$$
$$\times f^{p}(R_{ji})f^{q}(R_{ki}) + \sum_{i}^{N} F(\bar{\rho}_i), \tag{1}$$

where

$$\bar{\rho}_i = \sum_{j\neq i} \rho(R_{ji}), \tag{2}$$

and i, j, and k are indexes of interacting atoms.

In Eq. (1), the first term describes the sum of pairwise interactions depending on interatomic distances R_{ji}, the second term describes the sum of three-body interactions depending on interatomic distances R_{ji} and R_{ki} and bond angles θ_{jik}, and the last term describes the sum of higher-order interactions within the centrosymmetric approximation (CSA) [23].

The derivation of Eq. (1) is described in [23,24]. Here we only emphasize that $\Phi(R_{ji})$, $f^{p,q}(R_{ji})$, and $\rho(R_{ji})$ are only the basis functions with no physical meaning, while $g^{pq}(cos(\theta_{jik}))$ are the expansion coefficients of three-body interactions on basis functions $f^{p,q}(R_{ji})$. By varying the number n_3 of basis functions $f^{p,q}(R_{ji})$ the accuracy of three-body interactions can be tuned.

In a practical implementation of the interatomic potential, all basis functions are represented by cubic splines with equidistant knots. The values of the basis functions in the knots are optimizable parameters. The optimization of parameters is done by minimizing the value of the target function Z with a simulated annealing algorithm. The function Z is the weighted sum of deviations of values calculated with the interatomic potential from corresponding target values; see [23] for details. The target values usually include experimental data about cohesive energies, elastic constants, formation enthalpies, and theoretical data about energies, volumes, and forces in model lattices, and form a fitting database. By varying the weights of targets one can reach the desired accuracy of the interatomic potential for specific tasks or try to make it quite accurate in all tasks of atomistic modeling for the particular system.

2.2. Fitting database

To describe interatomic interactions in the Cr–Ta system, three potentials should be constructed within the N-body approach: one for Ta–Ta, one for Cr–Cr, and one for Cr–Ta interactions. To describe Cr–Cr interactions we used our already published potential [25]. The other two potentials were constructed within the N-body approach [23,24] in this work.

The *experimental* part of our fitting database for Ta–Ta interactions included cohesive (sublimation) energies, elastic constants (C_{11}, C_{12},

C_{44}), lattice parameters, and equation of state $P(V)$ of pure Ta in its ground-state body-centered cubic (bcc) structure. For fitting Cr–Ta interactions we did not use any experimental data due to their low availability.

The *theoretical* part of our fitting database for Ta–Ta interactions included energies and equilibrium volumes of model lattices (fcc, hcp, A15, C32, simple hexagonal and simple cubic), and energies and forces in two model bcc superlattices with 128 atoms. The configuration of the first superlattice was obtained by shifting one atom along the [001] direction on 0.05 Å. The configuration of the second superlattice was obtained after ab initio molecular dynamics simulation at 1100 K. The energies, volumes, and forces in model lattices were calculated within the density functional theory (DFT) using the projector-augmented wave (PAW) approach [26] for the treatment of core-valence electrons interactions and generalized-gradient approximation (GGA) in the form of Perdew–Burke–Ernzerhof (PBE) functional [27] for exchange–correlation energy as implemented in VASP [28]. We used value of 600 eV for plane-wave energy cutoff and density of k-points corresponding to the $30 \times 30 \times 30$ mesh for bcc cell of Ta with two atoms. The Methfessel–Paxton [29] smearing of the Fermi level with 0.3 eV smearing width was used. The chosen parameters of DFT calculations ensured the accuracy of 0.1 meV in the total energy calculations of the model lattices of Ta.

The theoretical part of our fitting database for Cr–Ta interactions included elastic constants, formation enthalpies, and volumes of several model lattices calculated within the PAW GGA approach. The Cr–Ta model lattices included 15 bcc solid solutions with concentrations from 6.25 to 93.75 at.% Cr and 22 lattices of Laves phases with C14 and C15 structures with and without deviations from stoichiometric Cr_2Ta composition.

2.3. Calculation details of diffusion coefficients

To estimate the influence of different diffusion mechanisms on diffusion coefficient in Cr_2Ta, we calculated the mean-squared displacements (MSD) of atoms in different model samples: (i) the ideal sample without defects, (ii) three samples (for getting the averaged quantities) with monovacancy in Cr position, and (iii) three samples with monovacancy in Ta position. The structures of model samples can be found in the Supplementary materials.

The MSD in the ideal sample gives us the estimation of the contribution of the interstitial mechanism into diffusion because in the lattices with elements of different radius the element with smaller atomic radius can move through interstitials of the host metallic lattice without need for creation of vacancies in the host lattice. Thus, calculating the MSD in the Laves phase without vacancies we can see if the atoms of smaller element (Cr) can move through the Cr_2Ta lattice in a similar way as carbon atoms move in carbides, for example. The MSD in samples with vacancies in Cr and Ta positions gives us the estimation of the influence of Cr and Ta vacancies on diffusion, respectively.

Because the contribution of vacancies depends on their concentration, the vacancy diffusion coefficients should be scaled with the following equation [25]:

$$D(T) = C^{vac}(T) \times N \times D_i^{vac1}(T), \tag{3}$$

where $C^{vac}(T)$ is the vacancy concentration at temperature T, N is the number of nodes in the simulation cell, and $D_i^{vac1}(T)$ is the diffusion coefficient calculated as a slope of the linear fit of MSD versus modeling time.

The vacancy concentration is determined as follows:

$$C^{vac}(T) = exp(-G^{vac}/k_BT) = exp(-H^{vac}/k_BT)exp(S^{vac}/k_B), \tag{4}$$

where G^{vac}, H^{vac}, and S^{vac} are the Gibbs free energy, enthalpy, and entropy of vacancy formation, respectively.

In our work, we consider the formation of vacancies in Cr_2Ta within the Schottky mechanism. Thus, the enthalpy and entropy of vacancy formation can be obtained as [30]:

$$H_{Cr}^{vac} = H_{Cr_{2n-1}Ta_n} - H_{Cr_{2n}Ta_n} \frac{3n-1}{3n}, \qquad (5)$$

$$S_{Cr}^{vac} = S_{Cr_{2n-1}Ta_n} - S_{Cr_{2n}Ta_n} \frac{3n-1}{3n}, \qquad (6)$$

for Cr vacancy, and:

$$H_{Ta}^{vac} = H_{Cr_{2n}Ta_{n-1}} - H_{Cr_{2n}Ta_n} \frac{3n-1}{3n}, \qquad (7)$$

$$S_{Ta}^{vac} = S_{Cr_{2n}Ta_{n-1}} - S_{Cr_{2n}Ta_n} \frac{3n-1}{3n}, \qquad (8)$$

for Ta vacancy, where $H_{Cr_{2n-1}Ta_n}$, $H_{Cr_{2n}Ta_{n-1}}$, $H_{Cr_{2n}Ta_n}$, $S_{Cr_{2n-1}Ta_n}$, $S_{Cr_{2n}Ta_{n-1}}$, and $S_{Cr_{2n}Ta_n}$ are the enthalpies and entropies of model Cr_2Ta supercells with vacancy in Cr and Ta positions, and of ideal supercell without vacancies, respectively. The enthalpy and entropy terms include temperature dependent vibrational contributions that where calculated in our work within the harmonic approximation as implemented in the Phonopy package [31].

3. Results

3.1. Results of fitting and testing interatomic potentials

In this work, we have constructed and tested several tens of interatomic potentials describing Ta–Ta and Cr–Ta interactions. Among these potentials, we have chosen those that reproduce the lattice parameters, point defect properties, and thermal stability of bcc Ta and C15 Cr_2Ta Laves phase in the best agreement with the experimental and DFT data. Further, we will refer to the chosen potentials for Ta–Ta and Cr–Ta interactions as POT_Ta and POT_CrTa, respectively. Tables A.1 and A.2 in Appendix A list arguments and values of the potential functions comprising the POT_Ta and POT_CrTa, while Figs. A.1 and A.2 illustrate the potential functions in graphical form. The files with the potentials and the example how to use them with LAMMPS package can be found in the Supplementary materials.

3.1.1. Accuracy of fitting

First of all, we estimated the accuracy of interatomic potentials in reproducing the target quantities used in fitting their parameters. In Table 1, the main characteristics of bcc Ta and Cr_2Ta in C15 structure calculated with POT_Ta and POT_CrTa are presented in comparison with experimental and DFT data.

As it is seen from Table 1, the constructed potentials reproduce lattice parameters and elastic moduli of bcc Ta in almost quantitative agreement with target experimental data and in a qualitative agreement with target DFT data. The maximum deviation of elastic constants calculated with POT_Ta from their corresponding experimental values is about 1%. There is also an excellent agreement of lattice parameter and cohesive energy of pure Ta with experimental data. The POT_CrTa predicts the mechanical stability of the C15 Cr_2Ta Laves phase in a qualitative agreement with DFT data since its shear moduli and the compression modulus have positive values. The values of the lattice parameter of Cr_2Ta predicted by POT_CrTa at 298 K and 0 K are about 1.1% and 1.0% larger than the value of the experimental lattice parameter at room temperature taken from [37], respectively. On the other hand, the value of the lattice parameter predicted by DFT at 0 K [34] is about 0.3% smaller than its experimental value. Thus, our potential POT_CrTa predicts the values of the lattice parameter of C15 Cr_2Ta in worse agreement with experimental data than the DFT.

Fig. 1 shows a comparison of the calculated dependence of pressure of bcc Ta on the relative volume with the equation of state $P(V/V_0)$ obtained from experimental data [38].

As can be seen from Fig. 1, the potential POT_Ta reproduces well the experimental data of the equation of state for the bcc lattice.

Table 1
Binding energy E_{coh}, lattice parameter a_0 at 298 K for experimental data and at 0 K (in parentheses) for DFT data, and elastic moduli C_{ij} at 0 K for bcc Ta and C15 Cr_2Ta.

Property	POT_Ta	Exp.	DFT (0 K)
E_{coh}, eV/atom	8.09	8.10[a]	–
a_0, Å	3.299	3.303[b]	(3.322)[c]
C_{11}, GPa	264.0	266.0[d]	265.0[e]
C_{12}, GPa	155.0	158.0[d]	158.0[e]
C_{44}, GPa	87.0	87.0[d]	69.0[e]

Property	POT_CrTa	Exp.	DFT (0 K)
a_0, Å	7.038 (7.033)	6.961[f]	(6.937)[c]
B, GPa	215.0	–	261.0[g]
C', GPa	80.4	–	81.3[g]
C_{11}, GPa	322.1	–	369.4[g]
C_{12}, GPa	161.4	–	206.8[g]
C_{44}, GPa	105.2	–	99.5[g]

[a]Ref. [32].
[b]Ref. [33].
[c]Ref. [34].
[d]Ref. [35].
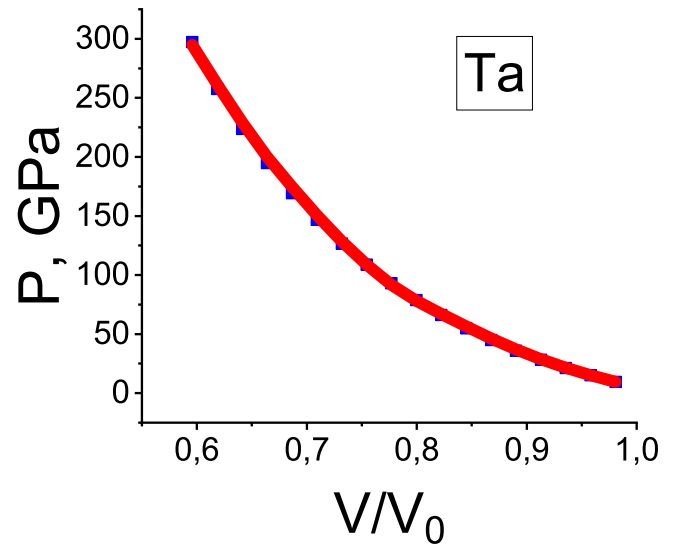[e]Ref. [36].
[f]Ref. [37].
[g]This work.

Fig. 1. Dependence of pressure P on the relative volume V/V_0 for the bcc Ta lattice. The dependence calculated using the POT_Ta potential is shown in red. The experimental data are taken from [38] and are shown in blue.

Table 2
The energies per atom ΔE of the model crystal lattices of A15, β-Ta, face-centered cubic (FCC), hexagonal close-packed (HCP), C32, simple cubic (SC) and simple hexagonal (SH) calculated using the potential POT_Ta in comparison with calculations by the DFT method. The energy of the equilibrium body-centered cubic (BCC) lattice is taken as the reference point.

Structure	ΔE, eV/atom	
	POT_Ta	DFT
A15	0.024	0.027
β-Ta	0.018	0.016
C32	0.258	0.223
FCC	0.144	0.250
HCP	0.284	0.286
SH	0.971	0.685
SC	1.326	1.106

Table 2 presents the results of calculations of the energies of a number of model lattices of Ta in comparison with the results of DFT calculations.
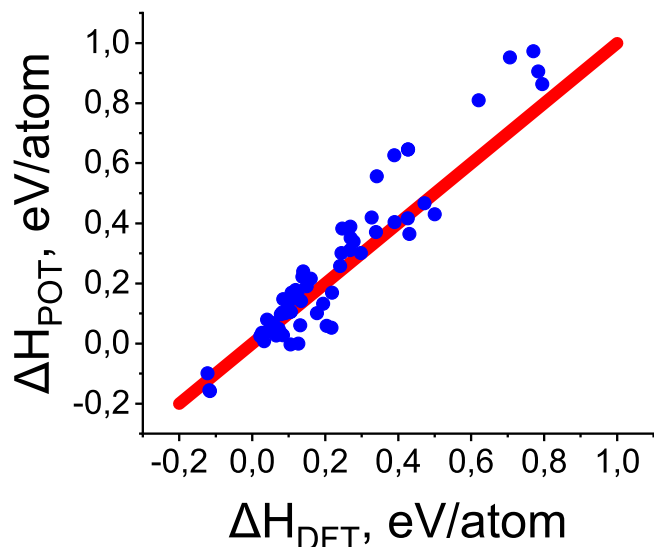
Fig. 2. Result of fitting the DFT data on the enthalpies of formation of model Cr–Ta lattices. The abscissa shows the values of the formation enthalpies of model Cr–Ta lattices, calculated within the DFT. The ordinate shows the enthalpies of formation of model Cr–Ta lattices, calculated using POT_CrTa.
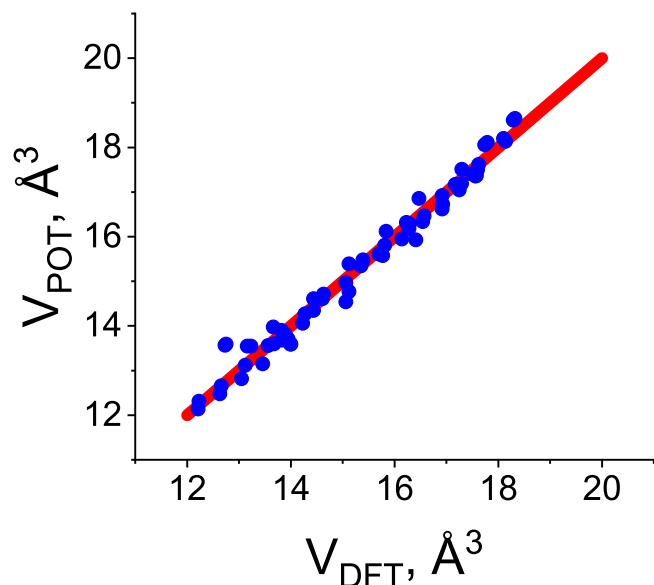

Fig. 3. Result of fitting the DFT data on equilibrium atomic volumes of model Cr–Ta lattices. The abscissa shows the values of the equilibrium atomic volumes of the model Cr–Ta lattices, calculated within the DFT. The ordinate shows the values of the equilibrium atomic volumes of the model Cr–Ta lattices, calculated using POT_CrTa.

As it can be seen from the data in Table 2, the energies of A15, β-Ta, FCC, HCP, C32, simple cubic (SC), and simple hexagonal (SH) crystal lattices, calculated using the potential for tantalum, lie higher than the energy of BCC lattice, meaning that the potential POT_Ta, correctly describe the BCC lattice as the most favorable one in terms of energy. There is also a qualitative agreement with the results of DFT calculations in the sequence of energies of the considered model lattices, except the energy of FCC lattice.

Figs. 2 and 3 show the results of fitting the formation enthalpies and equilibrium atomic volumes of the model Cr–Ta lattices, respectively.

All DFT values of the formation enthalpies of model Cr–Ta lattices, including solid solutions and Laves phases with non-stoichiometric composition, have a positive sign, except the enthalpies of formation of
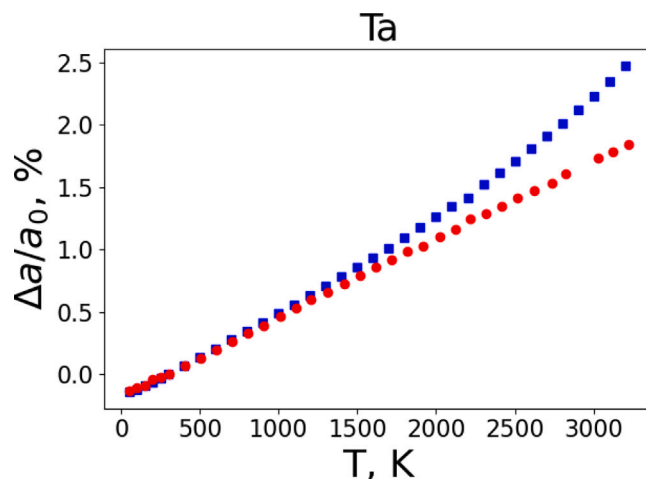

Fig. 4. The thermal expansion of pure Ta in bcc structure calculated with POT_Ta (red circles) in comparison with experimental data (blue squares) from [33].
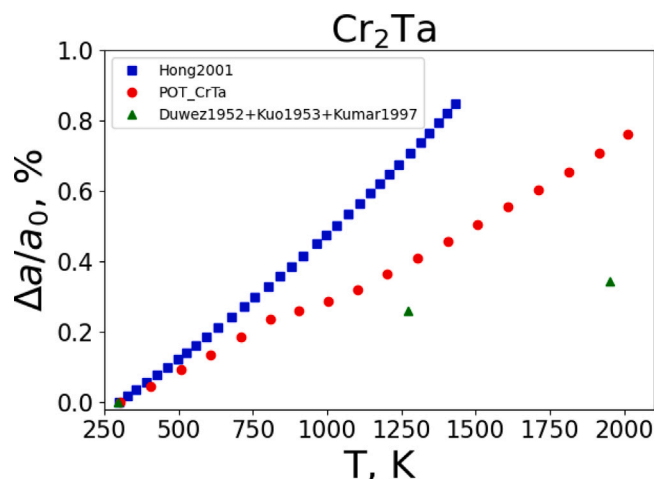

Fig. 5. The thermal expansion of Cr$_2$Ta in C15 structure calculated with POT_CrTa (red circles) in comparison with unpublished experimental data (blue squares) taken from the theoretical work (Hong2001 [17]) and with combined experimental data (green triangles) about the lattice parameters of C15 Cr$_2$Ta at room temperature (Duwez1952 [37]), 1273 K (Kuo1953 [39]), and between 1933 and 1968 K (Kumar1997 [40]).

C14 and C15 phases with stoichiometric composition Cr$_2$Ta. As can be seen from Figs. 2 and 3, POT_CrTa reproduces well the fitted formation enthalpies and equilibrium atomic volumes of model lattices, including two negative values for Laves phases with stoichiometric composition Cr$_2$Ta. It should be noted here that the calculated enthalpies of formation of solid solutions and Laves phases are in qualitative agreement with the phase diagram. According to the data on enthalpies of formation, Laves phases are present in the Cr–Ta phase diagram due to negative values of their enthalpies of formation and positive values of enthalpies of formation of Cr–Ta solid solutions. The presence of solid solutions in the Cr–Ta phase diagram can be explained by the contribution of the configurational entropy term to the Gibbs free energy.

3.1.2. Results of testing interatomic potentials

The second part in estimating the reliability of interatomic potentials is testing how they reproduce the properties that are not included in the fitting database. In Table 3, the defect properties of bcc Ta and Cr$_2$Ta in C15 structure calculated with POT_Ta and POT_CrTa potentials in comparison with available experimental and DFT data are shown.
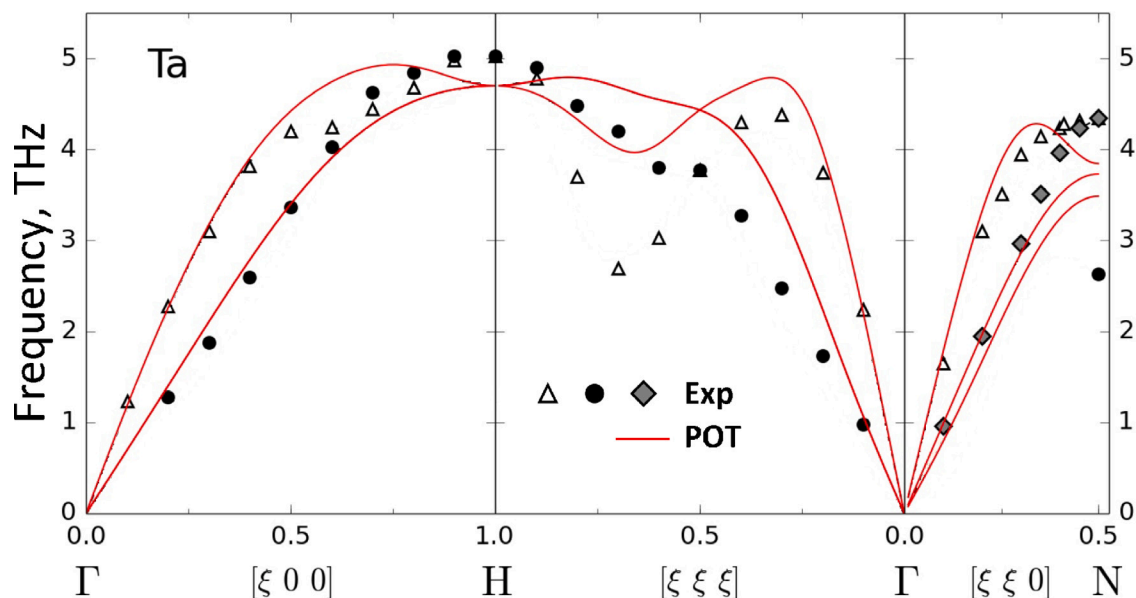
Fig. 6. Phonon dispersion curves of bcc Ta along the high symmetry directions of the Brillouin zone calculated using the POT_Ta potential (solid red lines) in comparison with experimental data [41] (triangles, circles, rhombuses).
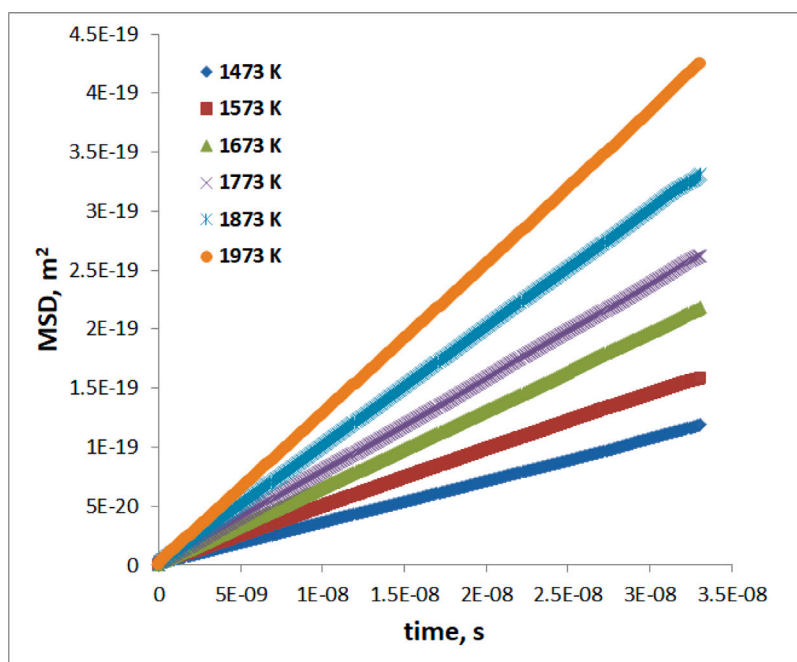

Fig. 7. The averaged dependencies of MSD from modeling time at temperatures from 1473 to 1973 K in the samples with vacancy in Cr position.

These properties were not included in the fitting database and can serve as a guide of how the interatomic potential will reproduce the diffusion properties.

From the data in Table 3, it can be seen that the values of the vacancy formation energy and the vacancy migration energy of bcc Ta obtained using our potential lie within the experimental error. The values of the activation energy for self-diffusion according to the vacancy mechanism given by POT_Ta are close to the experimental one. The dumbbell ⟨111⟩ has the lowest value of the formation energy among the interstitial atoms, which agrees with the results of DFT calculations. The formation enthalpies of Cr and Ta vacancies at 0 K and 0 GPa in Cr_2Ta C15 structure, $H_{Cr}^{vac}(0)$ and $H_{Ta}^{vac}(0)$, calculated according to Eqs. (5) and (8) are in qualitative agreement with the corresponding DFT values calculated in this work.

In Table 4, the melting point, melting heat of bcc Ta, and formation enthalpy of C15 Cr_2Ta Laves phase at 1693 K in comparison with available experimental data are presented. The melting point of bcc Ta was calculated from modeling the NPH (constant number of particles N, pressure P and enthalpy H) ensemble [46] in a two-phase superlattice with 19 652 atoms as it was done for W in our previous work [47]. One part of the superlattice consisted of the bcc phase while the other part consisted of the liquid phase. The heat of melting was calculated as the difference in the enthalpy of two superlattices one of which had the liquid structure while the other had the bcc structure at the determined melting point. The formation enthalpy of C15 Cr_2Ta Laves phase at a temperature T was calculated as follows:

$$\Delta_f H(T) = \frac{H_{Cr_2Ta}(T) - 2H_{Cr}(T) - H_{Ta}(T)}{3}, \tag{9}$$
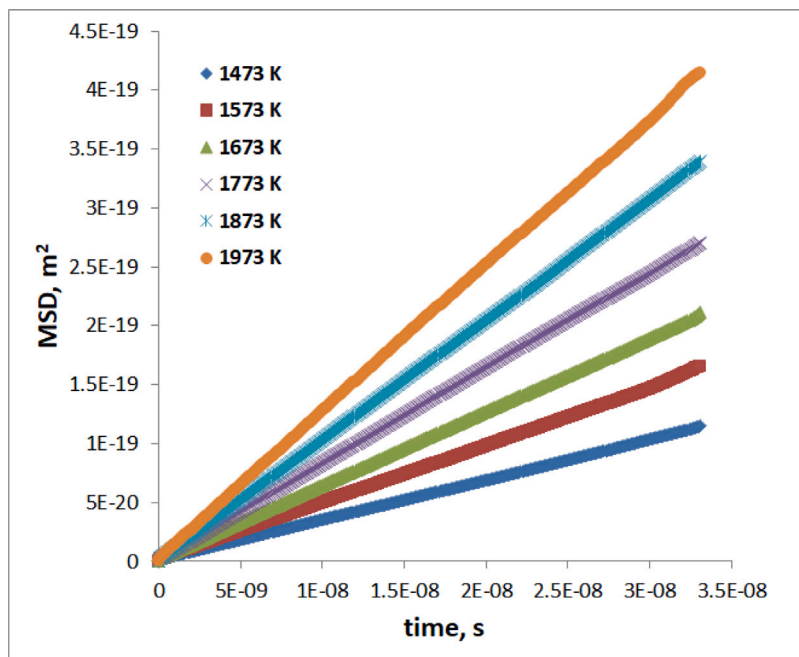
Fig. 8. The averaged dependencies of MSD from modeling time at temperatures from 1473 to 1973 K in the samples with vacancy in Ta position.
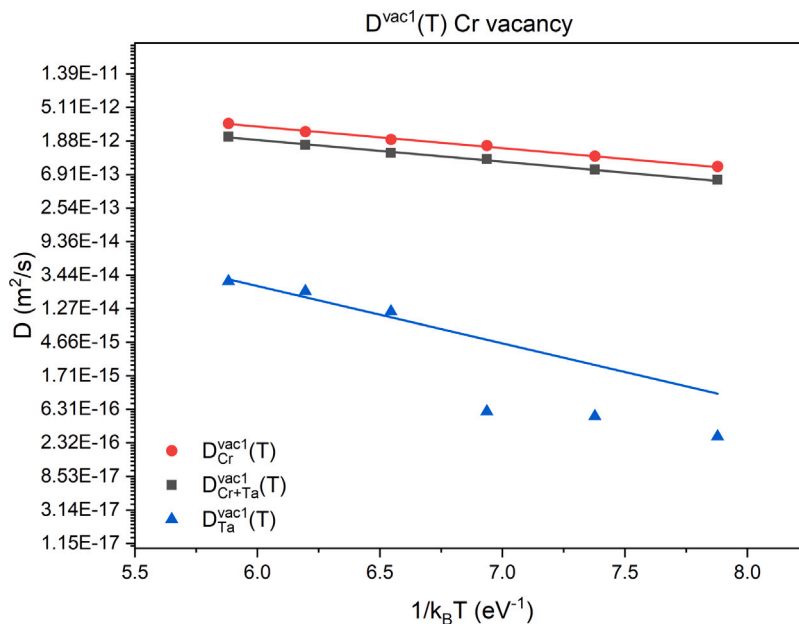

Fig. 9. The temperature dependence $D_i^{vac1}(T)$ calculated from MSD in model samples with the vacancy in the initial Cr position.

where $H_{Cr_2Ta}(T)$, $H_{Cr}(T)$, and $H_{Ta}(T)$ are the enthalpies of Cr_2Ta in C15 structure, Cr, and Ta in bcc structures, respectively, calculated by averaging the total energy over the last 20 000 timesteps after modeling the NPT (constant number of particles N, pressure P, and temperature T) ensemble at zero pressure.

From the data in Table 4, it can be seen that the value of the melting point calculated using the potential for tantalum coincides with the experimental value within the calculation error, while the melting heat calculated using the POT_Ta potential differs significantly from the experimental value by 49%. On the other hand, the calculated value of the formation enthalpy of C15 Cr_2Ta Laves phase at 1693 K is in good agreement with the corresponding experimental value [49].

In Figs. 4 and 5 the thermal expansions of bcc Ta and Cr_2Ta in C15 structure calculated with POT_Ta and POT_CrTa are shown in comparison with experimental data. The thermal expansions were calculated from a series of MD simulations at different temperatures using the NPT ensemble at zero pressure. During MD simulation at each temperature, the temperature was kept constant using Nose–Hoover thermostat [50,51] while the pressure was kept constant using Berendsen barostat [52].

As can be seen from Fig. 4, the potential POT_Ta predicts thermal expansion of bcc Ta in good agreement with the experimental data [33] up to a temperature of about 2000 K.

The experimental data about the thermal expansion of Cr_2Ta lattice is scarce. In the theoretical work of Hong et al. [17], the experimental data about the temperature dependence of thermal expansion coefficient of C15 Cr_2Ta is plotted along with the data calculated from the
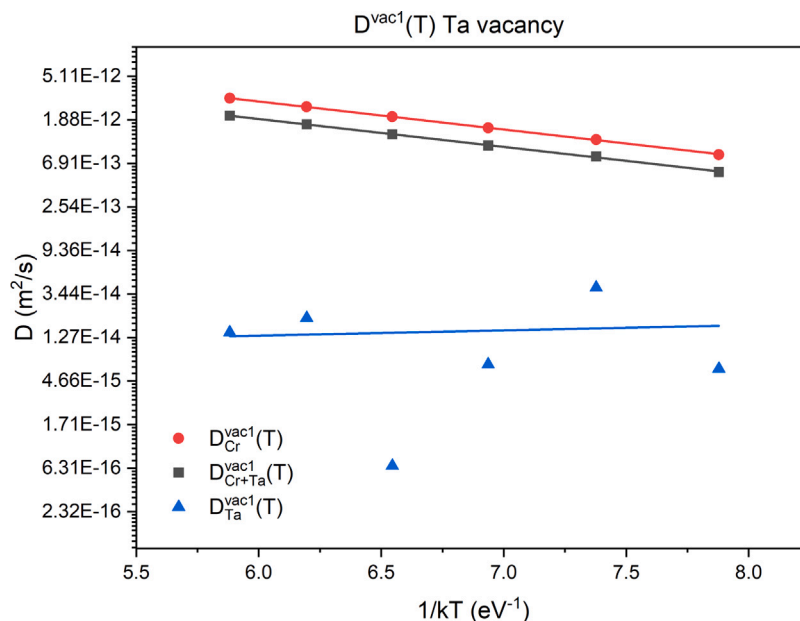
Fig. 10. The temperature dependence $D_i^{vac1}(T)$ calculated from MSD in model samples with the vacancy in the initial Ta position.
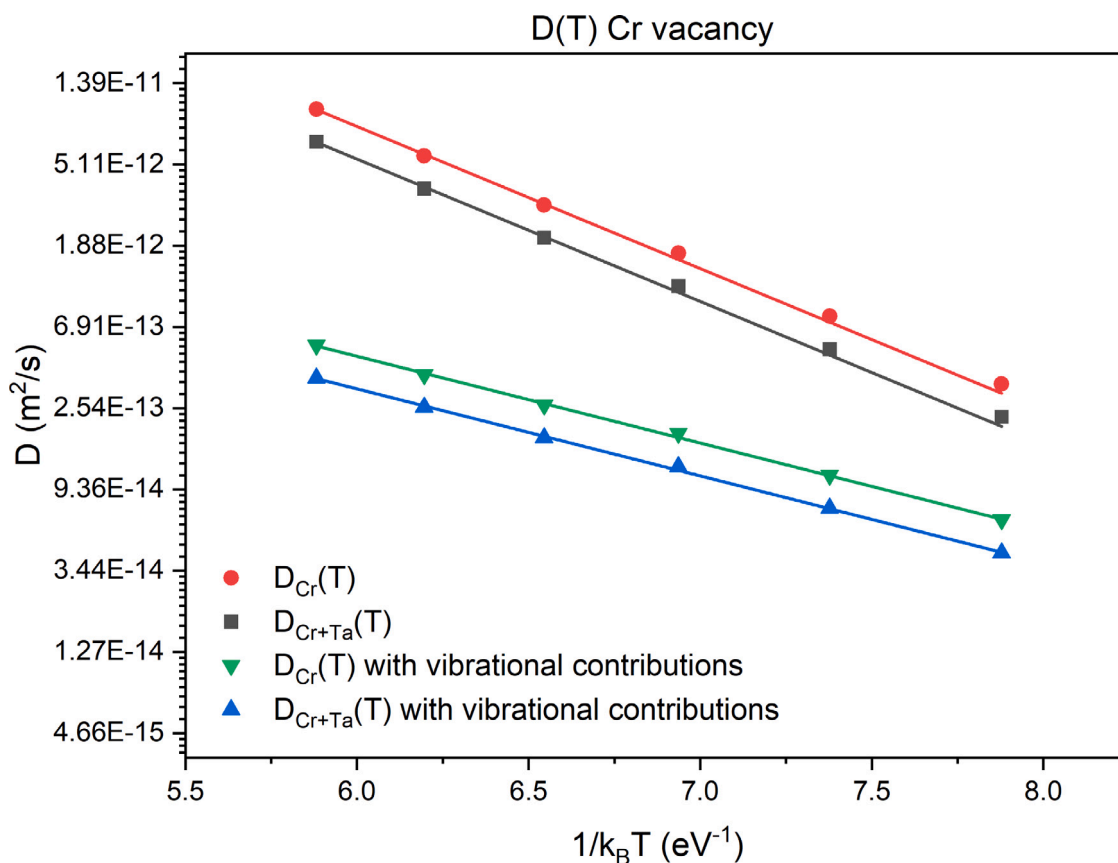

Fig. 11. The temperature dependence $D(T)$ calculated with Eq. (3) from MSD in model samples with the vacancy in the initial Cr position.

elastic constants obtained within the DFT. However, in [17] the experimental data is taken with the reference to the unpublished work, thus, their reliability is under question. Another way to get the information about the thermal expansion of C15 Cr_2Ta is to gain the experimental data about its lattice parameters at different temperatures that may be taken from the different sources. In literature, there are three experimental works [37,39,40] from which the lattice parameters of C15

Cr_2Ta at room temperature [37], 1273 K [39], and between 1933 and 1968 K [40] can be taken. Based on data from these works [37,39,40], another combined experimental set containing information about the thermal expansion of C15 Cr_2Ta at three temperatures can be created. From Fig. 5, it can be seen that the potential POT_CrTa predicts the thermal expansion of C15 Cr_2Ta lattice within the range of two different experimental sets.
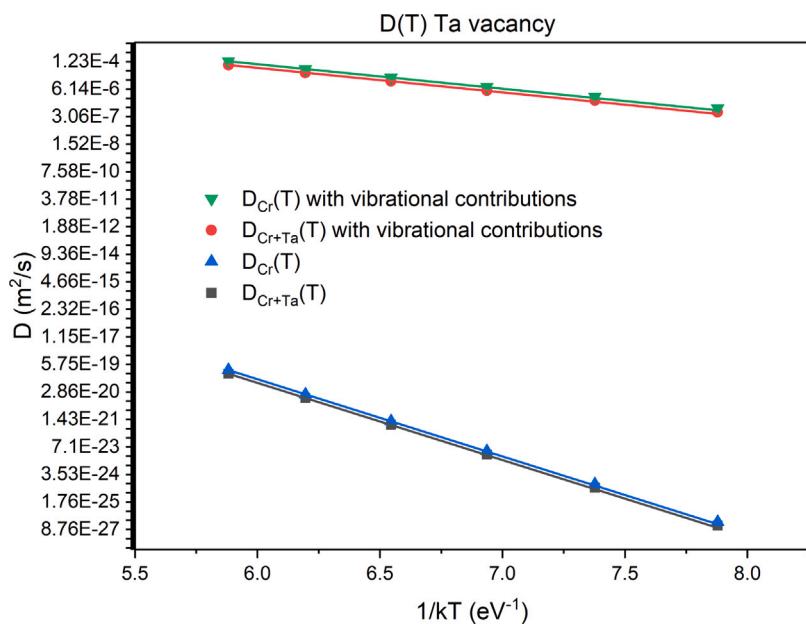
Fig. 12. The temperature dependence $D(T)$ calculated with Eq. (3) from MSD in model samples with the vacancy in the initial Ta position.
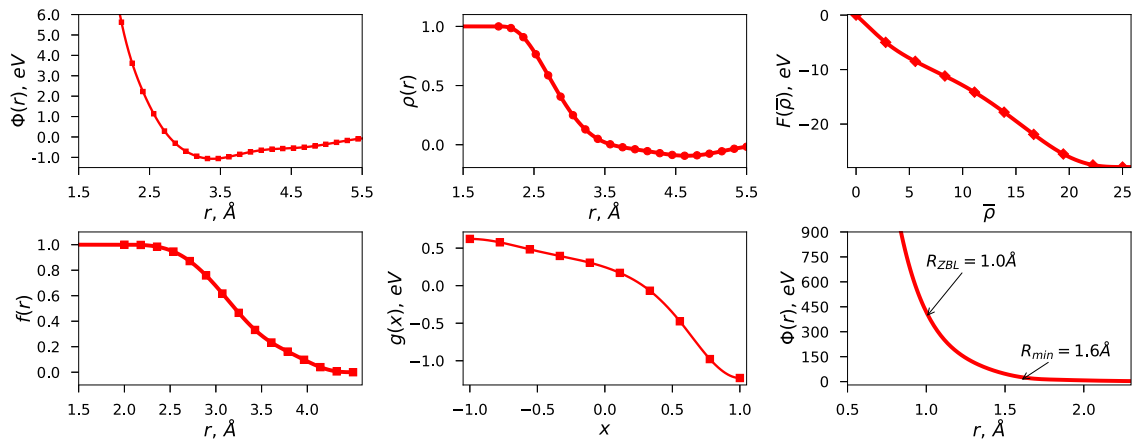
Fig. A.1. The potential functions in form of cubic splines describing interactions between Ta atoms in the POT_Ta potential. $\Phi(R)$ at $R < R_{ZBL}$ has the form of a Coulomb screened pair potential in Ziegler–Biersack–Littmark (ZBL) form [42] and is a fifth-degree polynomial in $[R_{ZBL}, R_{min}]$.
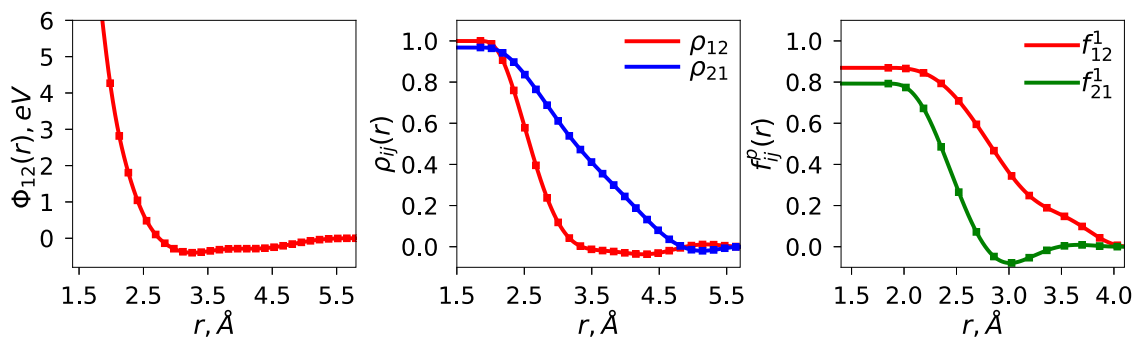
Fig. A.2. The potential functions in form of cubic splines describing cross interactions between Cr and Ta atoms in the POT_CrTa potential.

Table 3

Defect properties of bcc Ta and C15 Cr_2Ta in comparison with experimental and DFT data: $E^{vac}(0)$ - vacancy formation energy in bcc Ta at 0 K, E_v^m - vacancy migration energy, Q_v^{diff} - self-diffusion activation energy, $E_{\langle 110 \rangle}^f$, $E_{\langle 100 \rangle}^f$, $E_{\langle 111 \rangle}^f$, E_{oct}^f, and E_{tet}^f - interstitial atom formation energies, $H_{Cr}^{vac}(0)$ and $H_{Ta}^{vac}(0)$ - Cr and Ta vacancy formation enthalpies in Cr_2Ta C15 structure at 0 K calculated according to Eqs. (5) and (8).

Property	POT_Ta	Exp.	DFT
$E^{vac}(0)$, eV	2.99	2.20-3.10[a]	–
E_v^m, eV	1.29	0.70-1.90[a]	–
Q_v^{diff}, eV	4.28	3.56-4.12[b]	–
$E_{\langle 110 \rangle}^f$, eV	6.75	–	5.55[c]
$E_{\langle 100 \rangle}^f$, eV	6.92	–	6.04[c]
$E_{\langle 111 \rangle}^f$, eV	**6.03**	–	**4.82**[c]
E_{oct}^f, eV/atom	6.66	–	6.08[c]
E_{tet}^f, eV/atom	7.26	–	5.86[c]
Property	POT_CrTa	Exp.	DFT
$E_{Cr}^{vac}(0)$, eV/atom	1.051	–	1.716[d]
$E_{Ta}^{vac}(0)$, eV/atom	6.773	–	5.862[d]

[a]Ref. [43].
[b]Ref. [44].
[c]Ref. [45].
[d]This work.

Table 4

Melting point T_m, melting heat ΔH_m of bcc Ta, and formation enthalpy $\Delta_f H(1693)$ of C15 Cr_2Ta Laves phase at 1693 K in comparison with experimental data.

Property	POT_Ta	Exp.
T_m, K	3291 ± 20	3290[a]
ΔH_m, kJ/mol	18.7	36.6[a]
Property	POT_CrTa	Exp.
$\Delta_f H(1693)$, eV/atom	−0.088	−0.093[b]

[a]Ref. [48].
[b]Ref. [49].

Table A.1

Parameters specifying the cubic splines that comprise the potential functions of the POT_Ta. The first part of the table lists the number of knots N for each spline and the range of the spline variables t_{min} and t_{max}. The second part of the table gives the values at equally spaced spline knots defined by $t_i = t_{min} + (i-1)*(t_{max} - t_{min})/(N-1)$.

i	t	t_{min}	t_{max}	N
Φ	r (Å)	1.8	6.2	30
ρ	r (Å)	2.0	6.2	25
F	$\bar{\rho}$	0.0	25.0	10
f^1	r (Å)	2.0	4.5	15
g^{11}	x	−1.0	1.0	10

i	$\Phi(r_i)$ (eV)	$\rho(r_i)$	$F(\bar{\rho}_i)$ (eV)	$f^1(r_i)$	$g^{11}(x_i)$
1	12.35707499	1.00000000	0.00000000	1.00000000	0.62266212
2	8.59184587	0.98587865	−4.99614499	0.99814950	0.57723992
3	5.62628574	0.90887988	−8.48547576	0.98460629	0.48307245
4	3.61411410	0.76459257	−11.17487934	0.94616154	0.39583083
5	2.22604474	0.58633584	−14.13906125	0.87154397	0.30610401
6	1.13710227	0.40652175	−17.81561535	0.75889218	0.17043216
7	0.29143033	0.24956059	−21.88968284	0.61723756	−0.06730240
8	−0.30624073	0.12946259	−25.49263151	0.46571989	−0.47443181
9	−0.70021737	0.04953448	−27.50553953	0.33162758	−0.97767731
10	−0.94237038	0.00374371	−27.88212062	0.23302305	−1.22962748
11	−1.05711365	−0.02129224		0.16183130	
12	−1.05615745	−0.03818141		0.09766398	
13	−0.97175796	−0.05427488		0.03975243	
14	−0.85041315	−0.07141853		0.00633911	
15	−0.73533930	−0.08610671			
16	−0.64944525	−0.09303372			
17	−0.59698889	−0.08942609			
18	−0.56777289	−0.07563357			
19	−0.54266332	−0.05530090			
20	−0.50413140	−0.03418348			
21	−0.44265298	−0.01692710			
22	−0.35916878	−0.00598631			
23	−0.26404762	−0.00122060			
24	−0.17153138	−0.00007905			
25	−0.09513326				
26	−0.04230901				
27	−0.01301094				
28	−0.00182761				
29	0.00005600				
30	0.00000000				

In Fig. 6, the phonon dispersion curves of bcc Ta in comparison with experimental data are shown. The dispersion curves of the phonons were calculated with the PHONOPY package [31,53] using a 128-atom superlattice.

As it can be seen from Fig. 6, the potential POT_Ta predicts the phonon dispersion curves in the low-frequency region in good agreement with the experimental data. This is consistent with the good reproduction of the elastic constants of bcc Ta; see Table 1. On the whole, good agreement was obtained between the calculated and experimental values of frequencies along the symmetric directions of the Brillouin zone.

Summing up the results of testing of POT_Ta and POT_CrTa interatomic potentials, it can be concluded, that they should be suitable for modeling the diffusion in C15 Cr_2Ta Laves phase as they reproduce its point defect properties in a qualitative agreement with DFT data.

3.2. Results of calculation of diffusion coefficients in C15 Cr_2Ta

As it was mentioned in Section 2.3, to establish the diffusion mechanism and calculate diffusion coefficients in C15 Cr_2Ta Laves phase, we calculated MSD of atoms in model samples without any vacancies, with a vacancy in Cr position, and with a vacancy in Ta position of Cr_2Ta lattice in the temperature range from 1473 K to 2273 K with the step of 100 K. To calculate MSD, we used the samples with 1536 lattice nodes and anneal them for 30 ns with 2 fs timestep (15 000 000 timesteps) at each temperature using the NPT ensemble.

The analysis of MSD in the Cr_2Ta samples without vacancies showed us, that there is no diffusion in them at all temperatures in the studied range since after 30 ns annealing, the atoms in all model samples were displaced on distances not larger than interatomic distance.

In Figs. 7 and 8, the averaged dependencies of MSD from modeling time at temperatures from 1473 to 1973 K are shown for the samples with vacancies in Cr and Ta initial positions, respectively. At temperatures higher than 1973 K in some samples the dependence of MSD versus time was non-linear indicating that at these temperatures the phase transitions can take place. For this reason, we do not include the information about MSD obtained at temperatures higher that 1973 K for calculations of diffusion coefficients.

The analysis of MSD of atoms in the samples with vacancies in Cr and Ta initial positions showed us that diffusion coefficient $D_i^{vac1}(T)$ almost does not depend on sublattice where the vacancy was initially formed. In Figs. 9 and 10, the temperature dependencies $D_i^{vac1}(T)$ calculated from MSD of atoms in samples with vacancies in Cr and Ta initial positions are shown. It is seen that values of $D_{Cr+Ta}^{vac1}(T)$ and $D_{Cr}^{vac1}(T)$ are very close, while the values of $D_{Ta}^{vac1}(T)$ are several times smaller in both cases. This indicates that Ta atoms change their initial averaged positions much less than Cr atoms with time. Thus, it can be concluded that diffusion is governed by Cr atoms even in the case when Ta vacancy was initially formed. For this reason, we do not consider further the diffusion of Ta atoms as their contribution to the total diffusion is negligible.

To calculate $D(T)$ with the account of vacancy concentration, we used Eqs. (3) and (4). First, we estimated only enthalpic contribution to the vacancy concentration and diffusion coefficients using the values of $H_{Cr}^{vac}(0)$ and $H_{Ta}^{vac}(0)$ from Table 3 and neglecting the S^{vac} term in the Eq. (4). Then, we estimated the influence of temperature dependent vibrational contributions to the enthalpy and entropy of vacancy formation and hence vacancy concentration and diffusion coefficients.

Table A.2

Parameters specifying the cubic splines that comprise the potential functions of the POT_CrTa. The first part of the table lists the number of knots N for each spline and the range of the spline variables t_{min} and t_{max}. The second part of the table gives the values at equally spaced spline knots defined by $t_i = t_{min} + (i-1)*(t_{max}-t_{min})/(N-1)$.

i	t	t_{min}	t_{max}	N
Φ_{12}	r (Å)	1.7	5.8	30
ρ_{12}	r (Å)	1.85	5.8	25
ρ_{21}	r (Å)	1.85	5.8	25
f_{12}^1	r (Å)	1.85	4.2	15
f_{21}^1	r (Å)	1.85	4.2	15

i	$\Phi_{12}(r_i)$ (eV)	$\rho_{12}(r_i)$	$\rho_{21}(r_i)$ (eV)	$f_{12}^1(r_i)$	$f_{21}^1(r_i)$
1	8.74407469	0.99962800	0.96794558	0.86934085	0.79273299
2	6.31575439	0.98520800	0.96403037	0.86592476	0.77373160
3	4.26939431	0.90662479	0.94187066	0.84448387	0.67221968
4	2.81655397	0.75951217	0.89738398	0.79353993	0.48526428
5	1.80583658	0.57802046	0.83622624	0.70846169	0.26527993
6	1.04399929	0.39550257	0.76459600	0.59478365	0.07200324
7	0.48237976	0.23729700	0.68794381	0.46674765	−0.04760151
8	0.10412671	0.11825016	0.61122792	0.34391094	−0.07898482
9	−0.13688611	0.04220941	0.53859475	0.24870441	−0.05330146
10	−0.28763221	0.00319331	0.47218491	0.18927323	−0.01746897
11	−0.37193039	−0.01259398	0.41158005	0.14763072	0.00434013
12	−0.39820839	−0.01858253	0.35496217	0.09863457	0.00887985
13	−0.38255222	−0.02321099	0.29990336	0.04309324	0.00343669
14	−0.34781453	−0.02953124	0.24439589	0.00716443	0.00032983
15	−0.31496401	−0.03526146	0.18800401		
16	−0.29453814	−0.03623655	0.13209190		
17	−0.28736406	−0.03058735	0.07997140		
18	−0.28760149	−0.01916771	0.03606885		
19	−0.28559411	−0.00550371	0.00394800		
20	−0.27321684	0.00557808	−0.01443725		
21	−0.24666812	0.01094872	−0.01975644		
22	−0.20713709	0.01001523	−0.01549836		
23	−0.15998153	0.00507856	−0.00716980		
24	−0.11212442	0.00091102	−0.00122599		
25	−0.07022287				
26	−0.03819055				
27	−0.01688169				
28	−0.00517848				
29	−0.00065763				
30	0.00000000				

The obtained temperature dependencies of $D(T)$ with and without vibrational contributions on the concentration of vacancies are shown in Figs. 11 and 12.

The influence of lattice vibrations on vacancy formation has an opposite effect for Cr and Ta vacancy. If we do not take into account the lattice vibrations, the diffusion coefficient is several orders of magnitude higher if Schottky vacancy in Cr position is formed. The situation changes drastically with inclusion of vibrational contributions to the enthalpy and entropy of vacancy formation. Now, the main contribution to the diffusion in the C15 Cr_2Ta lattice is from Ta vacancies but governed by movement of Cr atoms.

Summarizing our findings, it can be concluded that the diffusion in the Cr_2Ta Laves phase with the C15 structure is mediated by Cr atoms which cannot move without initial creation of vacancies.

4. Conclusions

In this work, the interatomic potentials for modeling diffusion in the C15 Cr_2Ta Laves phase were constructed within the N-body approach [23] and thoroughly tested.

The potential for Ta–Ta interactions reproduces the lattice parameter, cohesive energy, elastic constants, equation of state, thermal expansion, point defect energies, and phonon dispersion of body-centered cubic Ta in qualitative agreement with DFT data and almost quantitative agreement with available experimental data in the temperature range of stability of C15 Cr_2Ta Laves phase.

The potential for Cr–Ta interactions reproduces the elastic constants, point defect properties, equilibrium volumes, and formation enthalpies of Cr–Ta structures in qualitative agreement with DFT data. Also, it reproduces the lattice stability and high-temperature formation enthalpy of C15 Cr_2Ta Laves phase in very close agreement with the available experimental data.

The calculations of diffusion coefficients with constructed potentials showed that diffusion in C15 Cr_2Ta lattice is governed by Cr atoms which cannot move without creation of vacancies.

The constructed potentials can be used in further investigations of diffusion processes in Cr–Ta phases at temperatures up to 2000 K, while the obtained results on diffusion coefficients in C15 Cr_2Ta Laves phase would be useful in the rational design of Cr–Ta based alloys.

CRediT authorship contribution statement

D.O. Poletaev: Writing – Original Draft, Formal analysis, Software, Investigation. **A.G. Lipnitskii:** Conceptualization, Supervision, Writing – Original Draft, Methodology, Software. **V.N. Maksimenko:** Investigation, Writing – Original Draft, Writing – review & editing , Visualization. **Yu.R. Kolobov:** Supervision, Conceptualization. **A.G. Beresnev:** Supervision, Conceptualization. **M.S. Gusakov:** Supervision, Conceptualization.

Declaration of competing interest

The authors declare that they have no known competing financial interests or personal relationships that could have appeared to influence the work reported in this paper.

Data availability

The authors confirm that the data required to reproduce the findings of this study are available within the article and in Supplementary materials and can be reproduced by any plotting and scientific visualization software and/or confirmed by DFT calculations. The Supplementary materials are available from https://data.mendeley.com/datasets/w2hx638sgn/1.

Appendix A. The potential functions describing Ta-Ta and Cr-Ta interatomic interactions

Tables A.1 and A.2 contain parameters specifying the cubic splines that comprise the potential functions of the POT_Ta and POT_CrTa.

Figs. A.1 and A.2 illustrate the potential functions of the POT_Ta and POT_CrTa in graphical form. They have smooth dependencies on the arguments, which indicates that there is no overflow in the number of optimized parameters with the used base of target values.

References

[1] N. Dupin, I. Ansara, Thermodynamic assessment of the Cr-Ta system, J. Phase Equilib. 14 (4) (1993) 451–456.

[2] J. Pavlů, J. Vřešťál, M. Šob, Re-modeling of laves phases in the Cr-Nb and Cr-Ta systems using first-principles results, Calphad: Comput. Coupling Phase Diagr. Thermochem. 33 (1) (2009) 179–186.

[3] Y. Jiang, S. Zomorodpoosh, I. Roslyakova, L. Zhang, Thermodynamic re-assessment of the binary Cr-Ta system down to 0 K, Int. J. Mater. Res. 110 (9) (2019) 797–807.

[4] A. Bhowmik, K.M. Knowles, H.J. Stone, Microstructural evolution and interfacial crystallography in Cr–Cr2Ta, Intermetallics 31 (2012) 34–47.

[5] A. Bhowmik, C.N. Jones, I.M. Edmonds, H.J. Stone, Effect of mo, al and si on the microstructure and mechanical properties of Cr–Cr 2 Ta based alloys, J. Alloys Compd. 530 (2012) 169–177.

[6] M. Brady, J. Zhu, C. Liu, P. Tortorelli, L. Walker, C. McKamey, J. Wright, C. Carmichael, D. Larson, M. Miller, W. Porter, Intermetallic reinforced Cr alloys for high-temperature use, Mater. High Temp. 16 (4) (1999) 189–193.

[7] K. Kumar, L. Pang, C. Liu, J. Horton, E. Kenik, Structural stability of the laves phase Cr2Ta in a two-phase Cr–Cr2Ta alloy, Acta Mater. 48 (4) (2000) 911–923.

[8] M.P. Brady, J.H. Zhu, C.T. Liu, P.F. Tortorelli, L.R. Walker, Oxidation resistance and mechanical properties of laves phase reinforced Cr in-situ composites, Intermetallics 8 (9–11) (2000) 1111–1118.

[9] A. Bhowmik, H.T. Pang, S. Neumeier, H.J. Stone, I. Edmonds, Microstructure and oxidation resistance of Cr-Ta-Si alloys, MRS Proc. 1295 (2011) 10–1295.

[10] A. Bhowmik, S. Neumeier, J.S. Barnard, C.H. Zenk, M. Göken, C.M. Rae, H.J. Stone, Microstructure and mechanical properties of Cr–Ta–Si laves phase-based alloys at elevated temperatures, Phil. Mag. 94 (34) (2014) 3914–3944.

[11] M. Brady, C. Liu, J. Zhu, P. Tortorelli, L. Walker, Effects of Fe additions on the mechanical properties and oxidation behavior of CrTa laves phase reinforced cr, Scr. Mater. 52 (9) (2005) 815–819.

[12] R. Tien, J. Zhu, C. Liu, L. Walker, Effect of Ru additions on microstructure and mechanical properties of Cr–TaCr2 alloys, Intermetallics 13 (3–4) (2005) 361–366.

[13] J. Yao, S.-q. Lu, X. Xiao, L.-p. Deng, Effect of molybdenum on the microstructure and oxidation behavior of hot-pressed TaCr2 alloys, Met. Sci. Heat Treat. 61 (3–4) (2019) 249–255.

[14] Y. Xue, S. Li, Y. Wu, C. Liu, H. Liu, L. Yuan, Strengthening and toughening effects in laves phase Cr2Ta/Cr in-situ composites by Si additions, Vacuum 174 (January) (2020) 109202.

[15] X.J. Liu, P. Yang, S.Y. Yang, J.J. Han, Y. Lu, Y.X. Huang, J.B. Zhang, C.P. Wang, Experimental investigations of phase equilibria in the Ta-V-Cr Ternary system, J. Phase Equilib. Diffus. 41 (6) (2020) 891–899.

[16] S. Hong, C. Fu, M. Yoo, Elastic properties and stacking fault energies of Cr2Ta, Intermetallics 7 (10) (1999) 1169–1172.

[17] S. Hong, C. Fu, Theoretical study on cracking behavior in two-phase alloys Cr–Cr2X (X=Hf, Nb, Ta, Zr), Intermetallics 9 (9) (2001) 799–805.

[18] B. Mayer, H. Anton, E. Bott, M. Methfessel, J. Sticht, J. Harris, P. Schmidt, Ab-initio calculation of the elastic constants and thermal expansion coefficients of laves phases, Intermetallics 11 (1) (2003) 23–32.

[19] A. Bhowmik, R.J. Bennett, B. Monserrat, G.J. Conduit, L.D. Connor, J.E. Parker, R.P. Thompson, C.N. Jones, H.J. Stone, Alloys based on Cr–Cr2Ta containing Si, Intermetallics 48 (2014) 62–70.

[20] Y.J. Bhatt, L. Kumar, R.V. Patil, G.B. Kale, S.P. Garg, Diffusion studies in Hf–Mo, Zr–Mo, Cr–Nb, Cr–Ta and Th–Re systems above 1900 k, J. Alloys Compd. 302 (1–2) (2000) 177–186.

[21] Q. Zhang, J.-C. Zhao, Impurity and interdiffusion coefficients of the Cr–X (X=Co, Fe, Mo, Nb, Ni, Pd, Pt, Ta) binary systems, J. Alloys Compd. 604 (2014) 142–150.

[22] K. Hachiya, Y. Ito, Molecular dynamics simulations of the self-diffusion phenomena in Ni2Y intermetallic phase, J. Alloys Compd. 279 (2) (1998) 171–178.

[23] A. Lipnitskii, V. Saveliev, Development of n -body expansion interatomic potentials and its application for V, Comput. Mater. Sci. 121 (2016) 67–78.

[24] A. Boev, I. Nelasov, V. Maksimenko, A. Lipnitskii, V. Saveliev, A. Kartamyshev, Molecular dynamics simulations of the excess vacancy evolution in V and V-4Ti, Defect Diffus. Forum 375 (2017) 153–166.

[25] V.N. Maksimenko, A.G. Lipnitskii, V.N. Saveliev, I.V. Nelasov, A.I. Kartamyshev, Prediction of the diffusion characteristics of the V-Cr system by molecular dynamics based on N-body interatomic potentials, Comput. Mater. Sci. 198 (June) (2021) 110648.

[26] P.E. Blöchl, Projector augmented-wave method, Phys. Rev. B 50 (24) (1994) 17953–17979.

[27] J.P. Perdew, K. Burke, M. Ernzerhof, Generalized gradient approximation made simple, Phys. Rev. Lett. 77 (18) (1996) 3865–3868.

[28] G. Kresse, J. Furthmüller, Efficiency of ab-initio total energy calculations for metals and semiconductors using a plane-wave basis set, Comput. Mater. Sci. 6 (1) (1996) 15–50.

[29] M. Methfessel, A. Paxton, High-precision sampling for Brillouin-zone integration in metals, Phys. Rev. B 40 (6) (1989) 3616–3621.

[30] S. Starikov, M. Korneva, Description of phase transitions through accumulation of point defects: UN, UO2 and UC, J. Nucl. Mater. 510 (2018) 373–381.

[31] A. Togo, I. Tanaka, First principles phonon calculations in materials science, Scr. Mater. 108 (2015) 1–5.

[32] C. Kittel, Introduction to Solid State Physics, eightth ed., John Wiley & Sons, Inc., 2005.

[33] K. Wang, R.R. Reeber, The role of defects on thermophysical properties: Thermal expansion of V, Nb, Ta, Mo and W, Mater. Sci. Eng. R 23 (3) (1998) 101–137.

[34] A. Jain, S.P. Ong, G. Hautier, W. Chen, W.D. Richards, S. Dacek, S. Cholia, D. Gunter, D. Skinner, G. Ceder, K.a. Persson, Commentary: The materials project: A materials genome approach to accelerating materials innovation, APL Mater. 1 (1) (2013) 011002.

[35] G. Simmons, H. Wang, Single Crystal Elastic Constants and Calculated Aggregate Properties: a Handbook, second ed., The MIT Press, Cambridge, 1971, p. 320.

[36] M. de Jong, W. Chen, T. Angsten, A. Jain, R. Notestine, A. Gamst, M. Sluiter, C. Krishna Ande, S. van der Zwaag, J.J. Plata, C. Toher, S. Curtarolo, G. Ceder, K.A. Persson, M. Asta, Charting the complete elastic properties of inorganic crystalline compounds, Sci. Data 2 (1) (2015) 150009.

[37] P. Duwez, H. Martens, Crystal structure of TaCr2 and CbCr2, JOM 4 (1) (1952) 72–74.

[38] R. McQueen, S. Marsh, J. Taylor, J. Fritz, W. Carter, The equation of state of solids from shock wave studies, in: R. Kinslow (Ed.), High-Velocity Impact Phenomena, Academic Press, New York and London, 1970, pp. 294–419.

[39] K. Kuo, Ternary laves and sigma-phases of transition metals, Acta Metall. 1 (6) (1953) 720–724.

[40] K. Kumar, C. Liu, Precipitation in a Cr-Cr2Nb alloy, Acta Mater. 45 (9) (1997) 3671–3686.

[41] A.D.B. Woods, Lattice dynamics of tantalum, Phys. Rev. 136 (3A) (1964) A781–A783.

[42] J.F. Ziegler, J.P. Biersack, The stopping and range of ions in matter, Treatise on Heavy-Ion Science: Volume 6: Astrophysics, Chemistry, and Condensed Matter, Springer US, Boston, MA, ISBN: 978-1-4615-8103-1, 1985, pp. 93–129,

[43] H. Schultz, Ta, in: H. Ullmaier (Ed.), Atomic Defects in Metals, in: Landolt-Börnstein - Group III Condensed Matter, vol. 25, Springer-Verlag, Berlin/Heidelberg, 1991, pp. 161–172.

[44] G. Neumann, V. Tölle, Self-diffusion in body-centred cubic metals: Analysis of experimental data, Phil. Mag. A 61 (4) (1990) 563–578.

[45] M.R. Fellinger, First Principles-Based Interatomic Potentials for Modeling the Body-Centered Cubic Metals V, Nb, Ta, Mo, and W (Ph.D. thesis), The Ohio State University, 2013.

[46] H.C. Andersen, Molecular dynamics simulations at constant pressure and/or temperature, J. Chem. Phys. 72 (4) (1980) 2384–2393.

[47] V. Maksimenko, A. Lipnitskii, A. Kartamyshev, D. Poletaev, Y.R. Kolobov, The N-body interatomic potential for molecular dynamics simulations of diffusion in tungsten, Comput. Mater. Sci. 202 (June 2021) (2022) 110962.

[48] A. Dinsdale, SGTE data for pure elements, CALPHAD 15 (4) (1991) 317–425.

[49] P. Feschotte, O. Kubaschewski, Thermochemical properties of the laves phase, Cr2Ta, Trans. Faraday Soc. 60 (1964) 1941.

[50] S. Nosé, A unified formulation of the constant temperature molecular dynamics methods, J. Chem. Phys. 81 (1) (1984) 511–519.

[51] S. Nosé, A molecular dynamics method for simulations in the canonical ensemble, Mol. Phys. 52 (2) (1984) 255–268.

[52] H.J.C. Berendsen, J.P.M. Postma, W.F. van Gunsteren, A. DiNola, J.R. Haak, Molecular dynamics with coupling to an external bath, J. Chem. Phys. 81 (8) (1984) 3684–3690.

[53] A. Togo, F. Oba, I. Tanaka, First-principles calculations of the ferroelastic transition between rutile-type and CaCl2-type SiO2 at high pressures, Phys. Rev. B 78 (13) (2008) 134106.